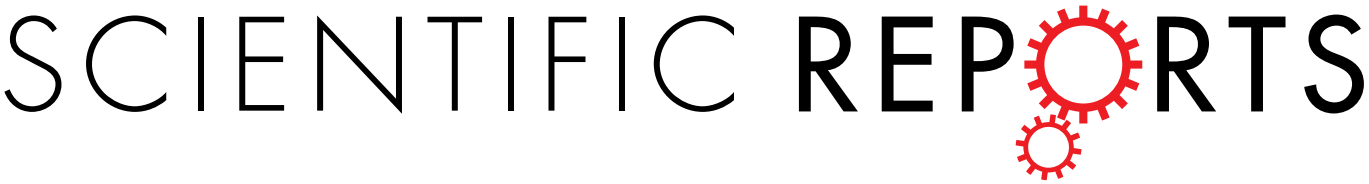

OPEN

Solar-light photocatalytic disinfection using crystalline/amorphous low energy bandgap reduced TiO_2

Received: 02 February 2016
Accepted: 08 April 2016
Published: 28 April 2016

Youngmin Kim, Hee Min Hwang, Luyang Wang, Ikjoon Kim, Yeoheung Yoon & Hyoyoung Lee

A generation of reactive oxygen species (ROS) from TiO_2 under solar light has been long sought since the ROS can disinfect organic pollutants. We found that newly developed crystalline/amorphous reduced TiO_2 ($rTiO_2$) that has low energy bandgap can effectively generate ROS under solar light and successfully remove a bloom of algae. The preparation of $rTiO_2$ is a one-pot and mass productive solution-process reduction using lithium-ethylene diamine (Li-EDA) at room temperature. Interestingly only the rutile phase of TiO_2 crystal was reduced, while the anatase phase even in case of both anatase/rutile phased TiO_2 was not reduced. Only reduced TiO_2 materials can generate ROS under solar light, which was confirmed by electron spin resonance. Among the three different types of Li-EDA treated TiO_2 (anatase, rutile and both phased TiO_2), the both phased $rTiO_2$ showed the best performance to produce ROS. The generated ROS effectively removed the common green algae *Chlamydomonas*. This is the first report on algae degradation under solar light, proving the feasibility of commercially available products for disinfection.

Around the globe, various parts of the regional aquatic ecosystems, including marine and fresh water, are being damaged by an increase in the frequency and severity of algal blooms, which are caused by natural phenomena or nutrient pollution from human activities such as agriculture, wastewater, and the use of fossil fuels. As we know, among the thousands of different algae, only a few species are known to be harmful and toxic. Harmful algal blooms like *Microcystis* and *Anabaena* can produce microcystins (cyanoginosins), which are dangerous toxins that can cause serious damage to the liver and/or sicken or even kill humans and animals[1,2]. Even though most algae are nontoxic, these species can also cause huge economic damage from fish kills, due to a competitively limited amount of oxygen in the water, as well as cause environmental problems if the algae are overgrown and massively accumulated in an aqueous medium. Most algae blooms lead to severely negative effects on the environment, economy, and public health[3]. Thus, to eliminate or reduce the algae blooms, there have been numerous approaches such as dilution and flushing, hypolimnetic withdrawal, activated sludge, phosphorus inactivation, oxidants (Cl_2, ClO_2), sediment oxidation, biomanipulation, and algicide (biocide) application ($CuSO_4$)[1,4]. However, these methods have not been significantly effective to reduce the algae blooms, and some methods cause secondary pollution to aquatic ecosystems by causing other problems or are culturally undesirable.

In recent decades, advanced photocatalyst semiconductors using physico-chemical processes have been applied with promising results for purification methods such as the removal of organic contaminants, deodorization, the disinfection of surfaces, and the removal of polluted air and water[2,3,5–9]. Studies on semiconductor materials that are abundant, stable, and efficient for photocatalytic reactions are still attracting interest worldwide because photocatalytic technology using solar energy has been considered to be a superior approach to solve both energy and environmental problems compared to other methods. Among many other semiconductor nanomaterials, titanium dioxide (TiO_2) is well known for its photocatalytic properties and is considered to be the most suitable candidate, mainly due to its cheapness, worldwide availability, chemical stability, high photocorrosion stability, and environmental friendliness[9,10]. TiO_2 also has good properties in charge transport, photo-electronic generation, light scattering, and energy conversion. When TiO_2 is irradiated by light that has a wavelength equal

Center for Integrated Nanostructure Physics, Institute for Basic Science, Department of Chemistry and Department of Energy Science, Sungkyunkwan University, Suwon 440-746, Korea. Correspondence and requests for materials should be addressed to H.L. (email: hyoyoung@skku.edu)

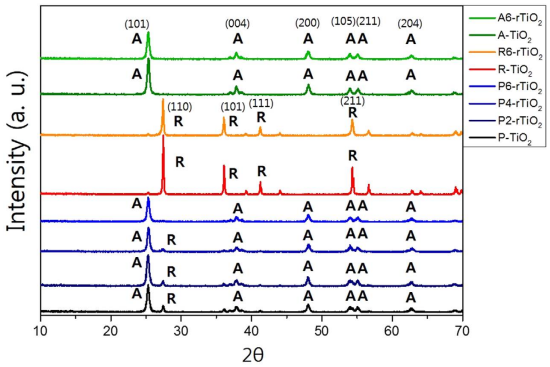

Figure 1. X-ray diffraction data of TiO_2 samples (P-TiO_2: pristine P25 TiO_2; P2-rTiO_2: TiO_2 after two days of being reduced; P4-rTiO_2: TiO_2 after four days of being reduced; P6-rTiO_2: TiO_2 after six days of being reduced; R-TiO_2: rutile phase only TiO_2; R6-rTiO_2: rutile phase only TiO_2 after six days of being reduced; A-TiO_2: anatase phase only TiO_2; A6-rTiO_2: anatase phase only TiO_2 after six days of being reduced).

to or smaller than its energy bandgap (3.2 eV or 387 nm), electron/hole pairs can be generated and can migrate to the crystalline surfaces. In the presence of oxygen, these electron/hole pairs can be reacted in an aqueous medium to generate reactive oxygen species (ROS), including hydroxyl radicals (OH·) and superoxide anions (O_2^{-}·), which are capable of degrading organic pollutants including algae and bacteria[11–14]. Despite its many advantages, conventional TiO_2 under a natural resource, such as sunlight, has intrinsically limited abilities for generating hydroxyl radicals (OH·) and superoxide anions (O_2^{-}·), mainly due to its large energy bandgap (3.2 eV or more), which leads to poor optical performance in the visible and near-infrared regions. This large energy bandgap characteristic of the conventional TiO_2 is the major drawback for its practical applications using sunlight. Thus, many researchers have struggled to overcome the large bandgap limitation of the conventional TiO_2 by applying different strategies such as doping with certain elements (cationic or anionic impurities)[11,15–17], using TiO_2 nanocomposites, and the bottom-up synthesis[18] of TiO_2 to control the nanocrystal structure or to modify its electronic band structure. Recently, hydrogenated TiO_2 (H-TiO_2) or black TiO_2 that is capable of absorbing visible and infrared light has gained much attention in the field of photocatalytic applications[19–21]. This H-TiO_2 shows superior performance in comparison with previous TiO_2 materials in terms of photocatalytic activity. The reduced energy bandgap property of the H-TiO_2 could be explained due to the formation of Ti-H and Ti-OH bonds and the high concentration of defects[22]. Despite its merits, the absorption enhancement has not been very effective regarding the visible-light photocatalytic activity. One of the greatest disadvantages for the use of the H-TiO_2 materials is the troublesome preparation method, which requires extreme reaction conditions using a high pressure (20 bars) hydrogen gas and a high reaction temperature.

Therefore, it is highly necessary to find a new way to prepare the low energy bandgap TiO_2 materials, including reduced TiO_2, under milder reaction conditions such as room temperature, and also to provide a method for mass production. It is expected that a low energy bandgap TiO_2 like a reduced TiO_2 (rTiO_2) material can effectively generate electrons/holes under sunlight, enhance the production of the ROS (1, 2), and as a result, effectively disinfect algae blooms. Unfortunately, to date there have been no reports on the killing or effective reduction of algae using the low energy bandgap TiO_2 under sunlight.

$$TiO_2 + hv \rightarrow e^- + h^+ \quad (1)$$

$$h^+ + H_2O \rightarrow \cdot OH + H^+ \quad (2)$$

Herein, we demonstrate the novel disinfection of freshwater algae using the crystalline/amorphous low energy bandgap rTiO_2 materials including a reduced rutile-only phased and both a crystalline anatase/amorphous reduced rutile-phased rTiO_2 (called HYL's rTiO_2) under a solar light system. First, we briefly introduce how to synthesize the HYL's rTiO_2 materials that are reduced with a solution-processible lithium-ethylenediamine (Li-EDA) solution at room temperature. Then, we report on the photocatalytic ability of the several HYL's rTiO_2 materials via the ROS generation with UV or solar or visible light irradiation and finally, on the disinfection of freshwater algae with sunlight, which can guide the practical environmental application for the reduction of algae blooms in freshwater rivers with our solar light system.

Results

Crystal structure characterization of TiO_2 samples. Figure 1 shows the XRD patterns of TiO_2 materials that were reduced over different reaction times (from two to six days). Rutile phase only TiO_2 (R-TiO_2) and anatase phase only TiO_2 (A-TiO_2), and their corresponding reduced samples after being reduced for six days (R6-rTiO_2 and A6-rTiO_2, respectively) are shown as well. The main peaks at 25.3°, 37.8°, 48.1°, 53.9°, 55.1°, and 62.7° correspond to the XRD pattern of the anatase phase, and the main peaks at 27.4°, 36.1°, 41.3°, and 54.3° correspond to the XRD pattern of the rutile phase[7,16,23,24]. The pristine P25 TiO_2 (P-TiO_2) and its corresponding reduced samples after being reduced for two days (P2-rTiO_2), four days (P4-rTiO_2), and six days (P6-rTiO_2) are shown. P-TiO_2 is known to contain both phases (anatase:rutile = 70~80%:30~20%). Surprisingly, when the

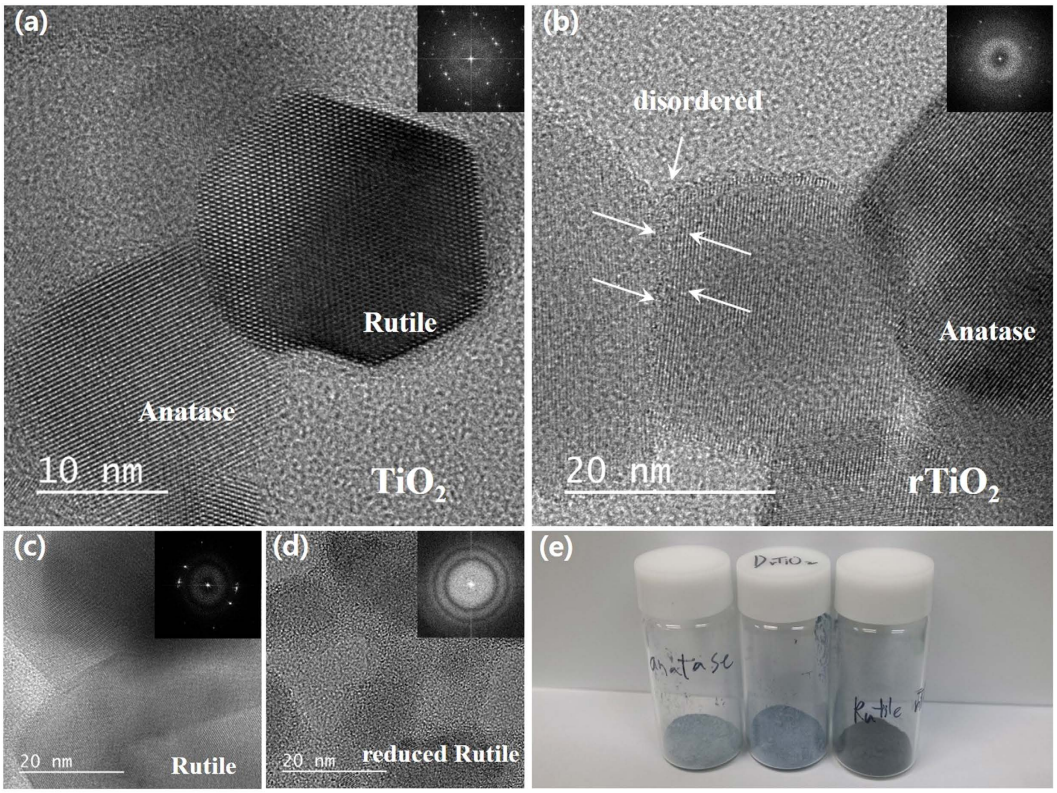

Figure 2. High resolution TEM images of TiO_2 samples. (**a**) Pristine P25 TiO_2 (P-TiO_2) showing an anatase-rutile interface, (**b**) TiO_2 after six days of being reduced (P6-rTiO_2) showing a disordered structure and ordered anatase phase, (**c**) rutile phase only TiO_2 (R-TiO_2) and (**d**) rutile phase only TiO_2 after six days of being reduced (R6-rTiO_2), with nanoparticles showing a disordered structure. (**e**) The photo images of anatase phase only TiO_2 after six days of being reduced (A6-rTiO_2, left), P6-rTiO_2 (middle), and R6-rTiO_2 (right).

P-TiO_2 was reduced by the Li-EDA to give HYL's rTiO_2, the peak intensities of the HYL's rTiO_2 at 27.4°, 36.1°, and 41.3° were decreased, which means that the rutile phase was reduced as the reaction time was increased. We like to refer that the possible mechanism on why the rutile phase is selectively (or easily) reduced in comparison to the anatase phase can be due to the large gap in the protonation constants between rutile phase and anatase phase against pH conditions[25]. We calculated the percentage of antase and rutile with various reaction times through the highest peak of each anatase phase peak (25.3°) and rutile phase peak (27.4°). The rutile % of P-TiO_2, P2-rTiO_2, P4-rTiO_2 and P6-rTiO_2 in comparison with anatase had 22.5, 16.6, 11.9 and 3.93%, respectively.

Figure 2(a–d) shows the high resolution TEM images of the TiO_2 samples, and the insets are the associated SAED patterns corresponding to each sample. The actual crystallite size of the P-TiO_2 was about 15 to 50 nm. We observed that the crystallinity of the P6-rTiO_2 and R6-rTiO_2 had been altered. The Li-EDA-treated reduction of the R-TiO_2 and P-TiO_2 caused the rutile phase region to become disordered so that the color of the R-TiO_2 turned black, like that of the H-TiO_2, while that of the anatase phase was changed only slightly. The TEM image of P-TiO_2 shows the well-defined anatase–rutile interface (Fig. 2a). However, the TEM image of the P6-rTiO_2 shows the contact boundary between the ordered and disordered TiO_2 nanoparticles (Fig. 2b). In Fig. 2c,d, we could observe dramatic changes in the rutile crystal structure after reduction. As a result, the colors of the A6-rTiO_2, R6-rTiO_2, and P6-rTiO_2 were all different. After reduction, a light blue color for the A6-rTiO_2, dark black color for the R6-rTiO_2, and deep blue color for the P6-rTiO_2 samples are shown in Fig. 2e, while all of them were white before being treated with Li-EDA.

Figure 3 shows the Raman spectra of P-TiO_2 and R-TiO_2. Those of P6-rTiO_2 and R6-rTiO_2 are also displayed. P-TiO_2 and P6-rTiO_2 showed almost the same peaks at 149, 400, 520, and 637 cm^{-1}, which are assigned to the E_g, B_{1g}, A_{1g} & B_{2g}, and E_{2g} modes of the anatase phase, respectively[25]. The Raman peaks of R-TiO_2 that are shown at 448 and 612 cm^{-1} were assigned to B_{1g} and B_{2g}, respectively. However, the Raman peaks of R-TiO_2 completely disappeared for the R6-rTiO_2 that was reduced by treatment with Li-EDA, which means that the molecular structure of the rutile phase was dramatically changed by the Li-EDA reducing agent.

Chemical properties of TiO_2 samples. Figure 4 shows the XPS spectra of the P-TiO_2, R-TiO_2, and A-TiO_2, as well as their reduced samples, P6-rTiO_2, R6-rTiO_2, and A6-rTiO_2. Each oxidation state was analyzed based on the Ti 2p and O 1s core levels to investigate the change in the chemical bonds of the P6-rTiO_2 compared to the P-TiO_2 sample. The original Ti 2p exhibited two peaks of 458.2 eV and 463.8 eV, which correspond to 2p3/2 and 2p1/2, respectively[26,27]. The P6-rTiO_2 revealed a similar behavior, but was shifted slightly toward the lower binding energy of Ti 2p peaks at 458.1 eV (2p3/2) and 463.7 eV (2p1/2). Both peaks are assigned to the Ti^{4+} oxidation

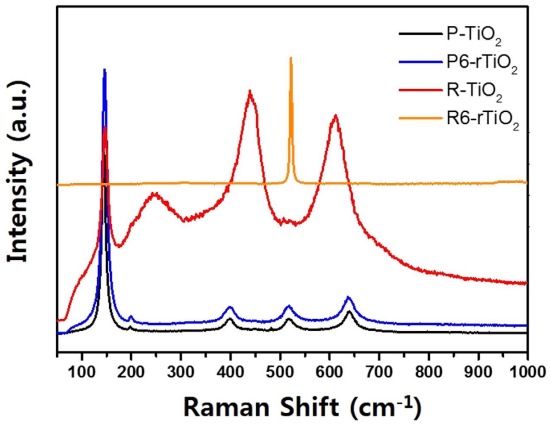

Figure 3. Raman spectra of pristine P25 TiO_2 (P-TiO_2) and rutile phase only TiO_2 (R-TiO_2) and their reduced samples (P6-rTiO_2 and R6-rTiO_2).

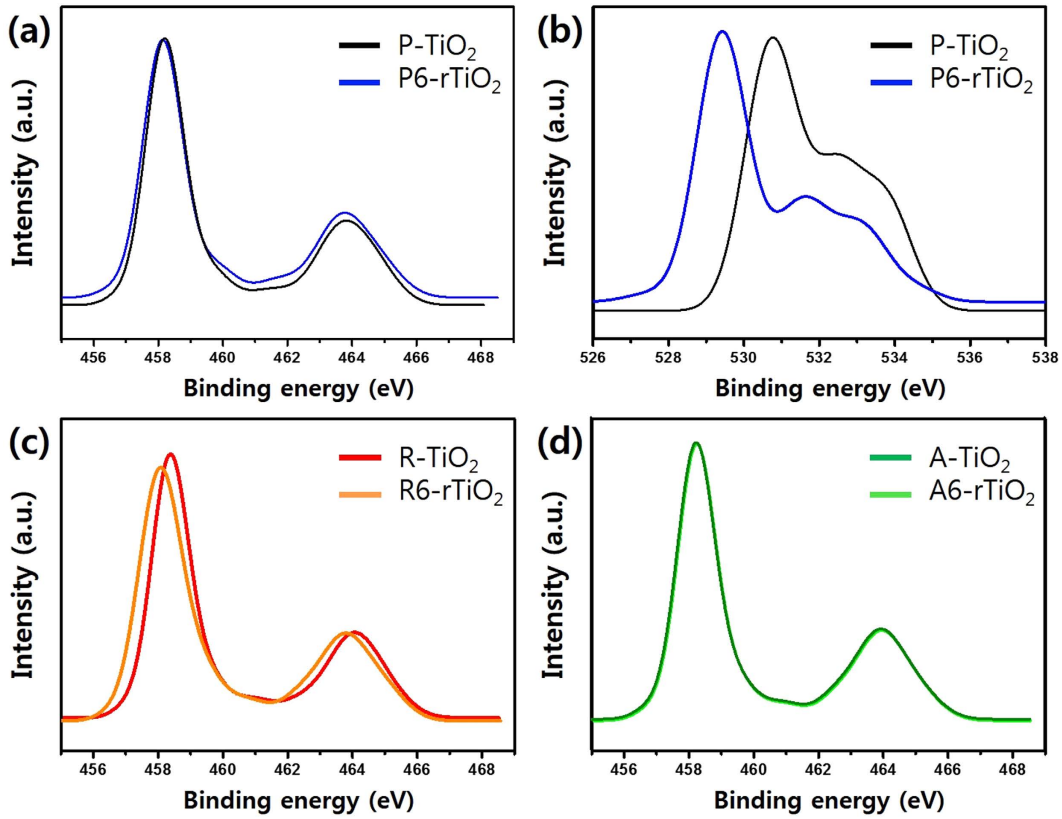

Figure 4. X-ray photoelectron spectra of TiO_2 samples. (**a,b**) Ti 2p and O 1s XPS spectra of the pristine P25 TiO_2 (P-TiO_2) and its reduced sample (P6-rTiO_2); (**c,d**) Ti 2p XPS spectra of the rutile phase only TiO_2 (R-TiO_2), anatase phase only TiO_2 (A-TiO_2), and their reduced samples (R6-rTiO_2 and A6-rTiO_2, respectively).

state in TiO_2 crystal, which is typical according to the previously reported XPS data[17,26,28,29]. However, the single O 1s peak, which can be assigned to the Ti-O bond at 530.7 eV of the P-TiO_2, was shifted to 529.4 eV (−1.3 eV) for P6-rTiO_2. This negative shift indicates that a different bonding environment such as oxygen vacancies occurred, making an electron negativity difference to the original value possible by the change in a surface chemical bond induced by the Li-EDA reduction. Surprisingly, the XPS peaks of the Ti 2p for A-TiO_2 and A6-rTiO_2 were almost identical, but the XPS peaks of the Ti 2p for the R-TiO_2 at 458.4 eV (2p3/2) and 464.1 eV (2p1/2) were negatively shifted to 458.1 eV (2p3/2) and 463.8 eV (2p1/2), respectively, which indicates that the reduction of TiO_2 with Li-EDA occurred only in the rutile phase, but not in the anatase phase of TiO_2. We also performed XPS survey

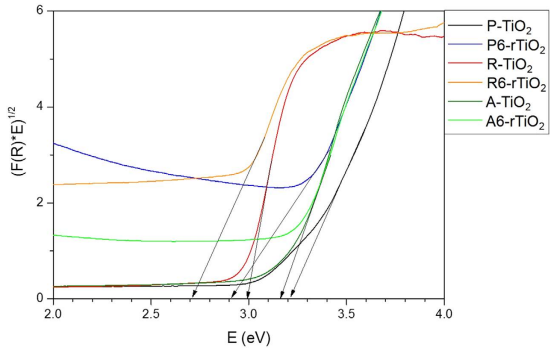

Figure 5. Transformed Kubelka—Munk function versus the photon energy graphs of the TiO_2 materials and their reduced TiO_2 samples.

scan spectra (see Supporting Information Figure S1) and EDS analysis of reduced TiO_2 samples (see Supporting Information Figure S2) to exclude the possibility of contamination such as Li or Cl in our samples.

To obtain a bandgap (Eg), the optical absorption of the TiO_2 nanomaterials is obtained from the UV-vis absorption spectra via a diffuse reflectance spectra using the Kubelka-Munk function,

$$F(R) = (1 - R)^2/2R(R: \text{reflectance}),$$

with the calculation of the photon energy given by $E = h\nu = 1240/\lambda$; the transformed Kubelka-Munk spectra are shown in Fig. 5. The dry TiO_2 powder sample was used to avoid difficulties, even though TiO_2 can be dispersed in solvent. The intersection between the linear fit and the photon energy (E, eV) axis gives the value of the bandgap (Eg)[17,30,31]. In this way, the bandgaps of the TiO_2 samples are indicated in Fig. 5. A reduction of the P-TiO_2 (Eg = 3.2 eV) gives the P6-rTiO_2 (Eg = 2.9 eV), and the R-TiO_2 (Eg = 3.0 eV) yields the R6-rTiO_2 (Eg = 2.7 eV). However, the bandgap reduction of the A-TiO_2 did not occur, and as a result, the bandgap was not changed (for A-TiO_2 and A6-rTiO_2, Eg = 3.16 eV). We also took Valence band XPS spectra of TiO_2 samples (see Supporting Information Figure S3) to estimate the valence band maxima. Thin black lines of each spectra show the linear extrapolation of the curves used for deriving the band edge position of TiO_2 samples. The valence band maxima of P-TiO_2, P3-rTiO_2, P6-rTiO_2, R-TiO_2 and R6-rTiO_2 are of 1.6, 1.8, 2.1, 1.9 and 2.2 eV below the Fermi energy, respectively. Considering the bandgap changes of each sample with the diffuse reflectance spectra, the proposed band diagram of TiO_2 samples are shown in Figure S4.

To investigate the photo-excitation and generation of the reactive oxygen radicals from the TiO_2 nanomaterials, ESR (also called electron paramagnetic resonance) was measured as shown in Fig. 6. The ESR spin-trap technique in water, accomplished using 5,5-dimethyl-1-pyrroline *N*-oxide (DMPO) as a spin trap[32] at room temperature, can detect the hydroxyl radical that is produced from the oxidation of water by the photogenerated holes from the TiO_2 nanomaterials[33]. All TiO_2 samples were prepared as follows. First, 5 mg of each TiO_2 powder were dispersed and sonicated in 4 ml of DI water in a small vial, and we then took 1 ml of the dispersion mixture, added approximately 4 μl of DMPO, placed the resulting combination into another small vessel, and vigorously shook it. The samples were irradiated for 5 min by a UV lamp or solar simulator. The spectra in Fig. 6a, in comparison with those in Fig. 6b,c, are of samples in a different solvent system in which ethanol was added (5 mg of each powder in 4 ml of mixed solvents, H_2O:EtOH = 5:1) to confirm the production of free hydroxyl radicals. The addition of ethanol quickly converted the hydroxyl radicals into carbon (C)-centered radicals. These spectra can be assigned to DMPO spin adducts of C-centered radicals[32]. The spectra in Fig. 6b of the samples in water under UV irradiation are composed of signals in a set with four characteristic peaks with the intensity ratio of 1:2:2:1, which are from hydroxyl radical spin adducts that are assigned to DMPO-•OH spin adducts[33,34]. ROS can be seen for all samples except the control, which is just DMPO in water (non). The ESR spectra for samples irradiated by the solar simulator in water are shown in Fig. 6c. Generally speaking, as the photons' energy decreased in the irradiation from the UV to the solar light system, the ESR peaks decreased or completely disappeared. This phenomenon is due to the fact that ESR spectra could be observed when the TiO_2 samples were irradiated with photons of energy exceeding the bandgap energy. In contrast, the intensity of the hydroxyl radicals increased as the surface oxygen vacancies increased, resulting in better photocatalytic activity. As a result, the R6-rTiO_2 and the P6-rTiO_2 (having both anatase and rutile phases) exhibited strong ESR peaks under solar light, but the other non-reduced TiO_2 samples and A6-rTiO_2 did not show any ESR signals as shown in Fig. 6c. We also checked ESR for R6-rTiO_2 and the P6-rTiO_2 under visible radiations at 410 and 510 nm using bandpass filter (XBPA410, XBPA510 bandpass filter, UniNanoTech Co., Ltd.) as shown in Fig. 6d. The reduced R6-rTiO_2 and the P6-rTiO_2 samples showed trace of radical peaks, but the radical peaks of the non-reduced samples were hardly observed. In a partial conclusion, with the active visible light of the solar light, the R6-rTiO_2 and the P6-rTiO_2 can generate the ROS, which is directly applicable for our global environmental problems.

Algae disinfection property of rTiO_2. Figure 7 illustrates the image of the experimental setup and the photocatalytic activity of the rTiO_2, as detailed in the Experimental Section, and Table 1 shows the experimental conditions for the TiO_2 samples. The photo-activity of all TiO_2 samples was evaluated by observing the

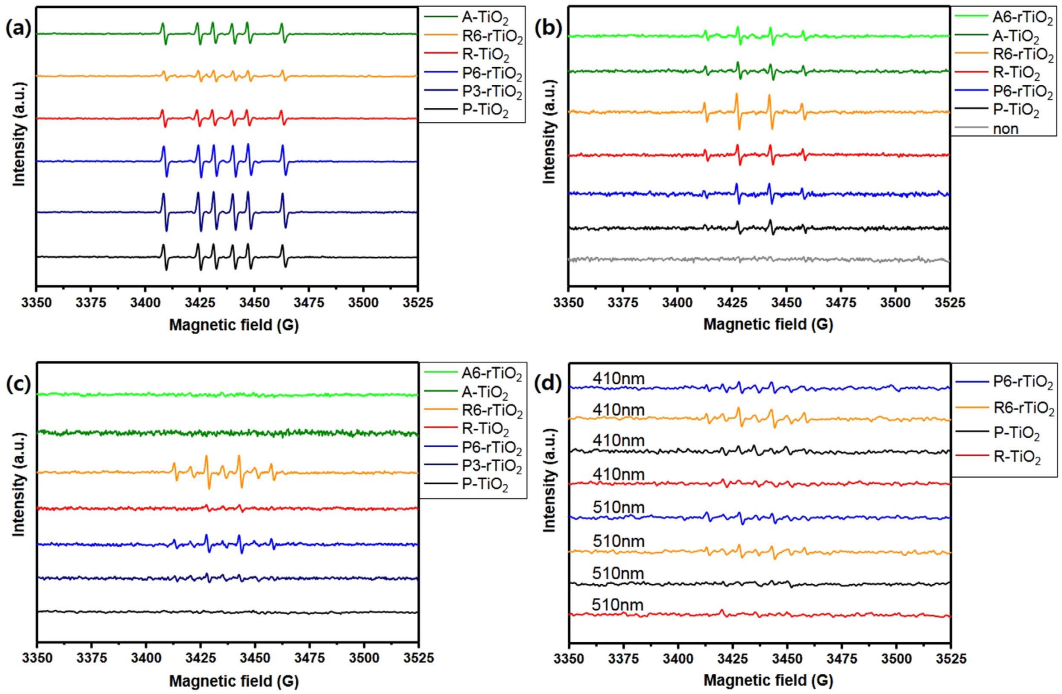

Figure 6. Electron spin resonance data of each TiO_2 sample under different conditions (A-TiO_2: anatase phase only TiO_2; A6-rTiO_2: anatase phase only TiO_2 after six days of being reduced; R-TiO_2: rutile phase only TiO_2; R6-rTiO_2: rutile phase only TiO_2 after six days of being reduced; P-TiO_2: pristine P25 TiO_2; P3-rTiO_2: TiO_2 after three days of being reduced; P6-rTiO_2: TiO_2 after six days of being reduced) (**a**) in ethanol and water co-solvent (H_2O:EtOH = 5:1) under UV irradiation, (**b**) in water under UV irradiation, (**c**) in water under solar irradiation, and (**d**) in water under irradiations at 410 and 510 nm wavelength using XBPA410, XBPA510 bandpass filter, UniNanoTech Co., Ltd.

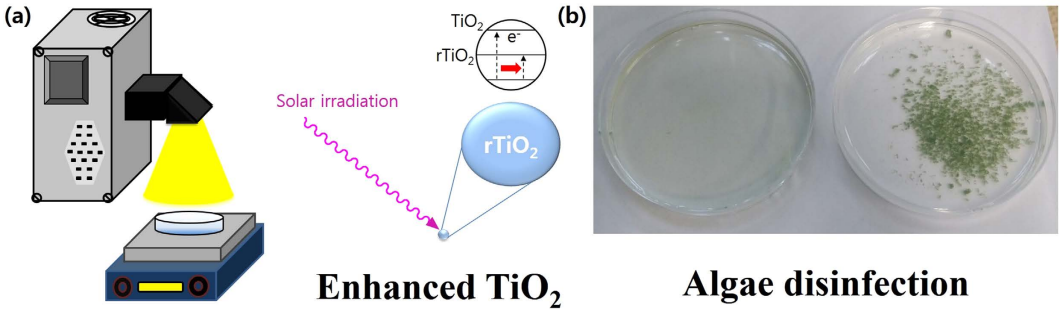

Figure 7. (**a**) The photocatalytic activity of reduced TiO_2 and its experimental setup. (**b**) Two petri dishes containing algae samples before (left, well dispersed) and after (right, aggregated and precipitated) the disinfection with reduced TiO_2.

Entry	Catalyst
1	Only Algae[b]
2	Algae + P-TiO_2
3	Algae + P6-rTiO_2
4	Algae + R-TiO_2
5	Algae + R6-rTiO_2
6	Algae + A-TiO_2
7	Algae + A6-rTiO_2

Table 1. Algae elimination reaction conditions[a]. [a]Reactions were carried out with each sample (10 mg, 0.125 mmol) in 20 ml of water with 4 h of stirring at room temperature under UV or solar irradiation. [b]5 ml of suspension were added; initial concentration was 7500 ± 10 cells/ml.

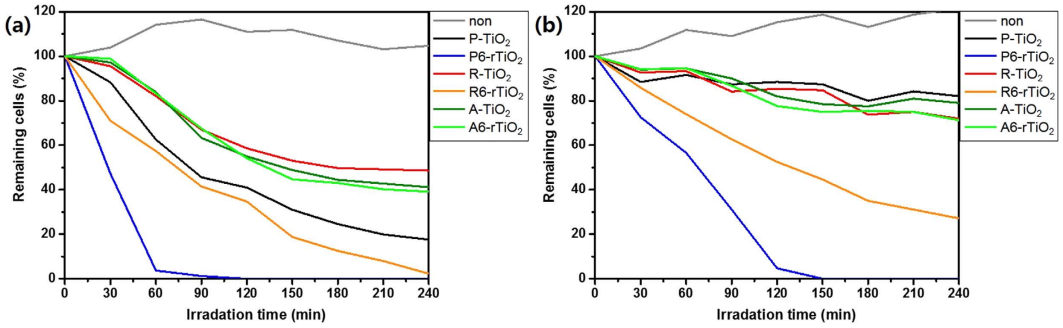

Figure 8. Photocatalytic degradation graph comparison of algae with each TiO_2 sample after exposure to (**a**) UV light or (**b**) solar light.

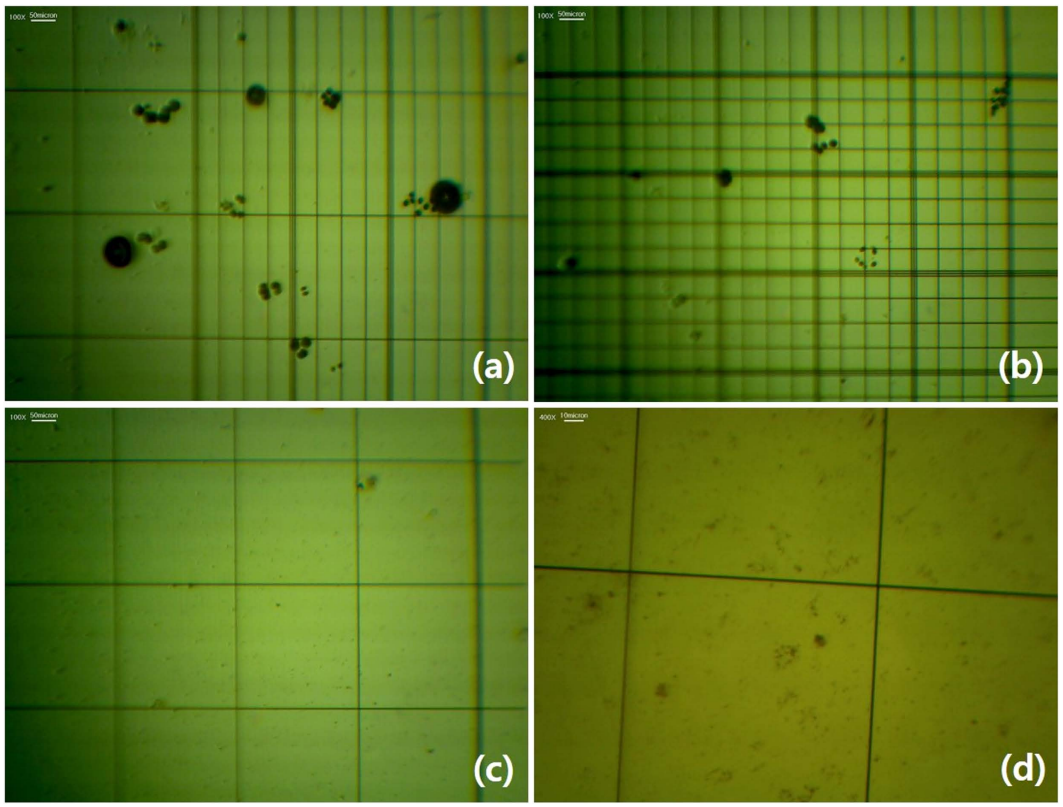

Figure 9. Optical microscope images with haemacytometers of algae that are alive (**a,b**) and that have been fully eliminated (**c,d**).

degradation of a *Chlamydomonas segnis* (*Lobochlamys segnis,* NLP Co., Ltd) suspension under UV light or solar light irradiation, as shown in Fig. 8. In Fig. 8a, after 4 h of UV irradiation, the percentages of cells remaining for the control (non, only algae), P-TiO_2, R-TiO_2, R6-rTiO_2, A-TiO_2, and A6-rTiO_2 were 104.7, 17.5, 48.6, 2.3, 41.1, and 39.1%, respectively. The percentage of remaining cells is compared to the initial number of algal cells. The R6-rTiO_2 degraded 50% of the cells after 1.5 h and had degraded almost all of them after 4 h. Amazingly, the P6-rTiO_2 had almost fully degraded the algae cells after 1 h and had completely degraded them after 2 h, while the P-TiO_2 degraded 60% of the algae. In Fig. 8b, after 4 h of solar irradiation, the percentages of cells remaining for the non, P-TiO_2, R-TiO_2, R6-rTiO_2, A-TiO_2 and A6-rTiO_2 samples were 121.5, 82.1, 72.0, 27.1, 79.0, and 71.3%, respectively. The R6-rTiO_2 had degraded about 50% after 2 h, whereas most of the other TiO_2 samples showed a low activity. Surprisingly, P6-rTiO_2 had almost fully degraded the algae after 2 h and had completely degraded them after 2.5 h. In fact, the unreduced samples, such as P-TiO_2, R-TiO_2, and A-TiO_2, were active only under UV light, but were not effective under solar light. However, the Li-EDA-treated TiO_2 (P6-rTiO_2 and R6-rTiO_2) showed effectiveness, even under solar light. In partial conclusion, the photocatalytic activities of the TiO_2 samples sharply increased with Li-EDA reduction, but only the P6-rTiO_2 nanomaterial could completely kill the algae under UV, and even under solar light. These breakthrough photocatalytic performances can be easily

explained due to the reduced TiO_2 nanomaterials that permit the creation of oxygen vacancies (defects) that work as trapped holes[3,18,35], leading to the lower recombination of electrons and holes, even with the low energy bandgap irradiation. In addition, the R6-rTiO_2, which has a lower energy bandgap (2.7 eV) than that of the P-TiO_2 (3.2 eV), could generate electrons, even with the low-energy irradiation such as solar light, which is composed of most visible and infrared wavelengths as well as UV light. As a result, the newly generated electrons can produce ROS and effectively degrade the algae under sunlight. Without the low energy bandgap of rTiO_2, the electrons could not be produced under the relatively weaker solar light. Furthermore, we found that the TiO_2 samples containing both reduced rutile and anatase phases exhibited higher catalytic activity than that of the one-phase TiO_2 samples, including the R6-rTiO_2 or A6-rTiO_2. This may be because the reduced rutile phase part of P6-rTiO_2 that has an irregular and disordered phase easily generates electrons/holes under solar light, and simultaneously, the unreduced anatase crystalline phase part of P6-rTiO_2 can enhance the charge separation of the electrons/holes by quickly transporting the electrons or the holes[19,35,36]. The possible mechanism about the charge transportation and separation efficiency was already reported in our group with the time-correlated single-photon counting (TCSPC) and PL experiments. TCSPC result revealed that the disordered/ordered TiO_2 phases gave the highest exciton separation and enhanced photo-catalytic process, and also PL quenching schematic illustration showed Li-EDA treatment can critically block the electron loss by obstructing the recombination[25]. This phenomenon is more effective under solar light irradiation. As a result, both the reduced irregular rutile phase and the unreduced anatase crystalline phase perform best for the disinfection of algae blooms even under sunlight, which is the first time that TiO_2 has been used for the disinfection of algae under sunlight, which can be applicable to our rivers under real-world conditions. These remarkable optoelectronic properties of rTiO_2, which has both reduced rutile and unreduced anatase phases, could provide valuable insight for various applications such as solar cells, electronic devices, and photocatalysis.

Discussions

The analysis of XRD, TEM and Raman clearly demonstrate the crystallinity change of rTiO_2 and the analysis of XPS, DRS and ESR show large differences especially regard to chemical properties and as a photocatalyst.

In conclusion, we demonstrated the simple room temperature one-pot synthesis of reduced TiO_2 from pristine TiO_2. This synthetic method could also be used in mass production, and the resulting reduced TiO_2 was composed of both disordered rutile and ordered anatase phases. The reduced TiO_2 showed the highest photo-activity not only under UV irradiation, but also under solar irradiation in the generation of reactive oxygen radicals, such as hydroxyl radicals that are capable of disinfecting algae. Thus, the reduced TiO_2 is superior to previously reported TiO_2 nanoparticles in generating ROS at lower energy levels. We assume that this improved photocatalytic performance is due to the oxygen defects of the TiO_2 surface that functioned as trapped holes, leading to a lower recombination of electrons and holes with a reduction of their bandgap. We also found the multi-phase TiO_2 to have better catalytic activity than the mono-phase TiO_2, especially under solar light irradiation. For this reason, we found that the multi-phase rTiO_2 was more effective for the degradation of algae than the single phase crystal forms of TiO_2, because the electrons generated from the reduced rutile part easily moved to the anatase part of TiO_2, leading to the higher production of ROS and resulting in better disinfection of the algae. This phenomenon was more apparent under sunlight than it was under UV light. Furthermore, rTiO_2 nanomaterials, having a small band gap in comparison with normal TiO_2, can be applied in various optoelectronic devices, including photovoltaic cells and other energy applications.

Methods

Materials and preparation of reduced TiO_2. Pristine TiO_2 was purchased commercially from Degussa (P25); lithium (Li) and ethylenediamine (EDA) were purchased from Sigma Aldrich. The purchased reagents were used directly with no further purification. The rTiO_2 nanoparticles were prepared as follows: 500 mg of TiO_2 (10 mg/ml) powder were dispersed in 50 ml of ethylenediamine, and then Li (0.347 g) was added to make a concentration of 1 mol/L. The solution was sonicated for 15 min and stirred at room temperature for two to six days. All of the procedures were done in anhydrous and nitrogen atmosphere conditions. As the reaction proceeded, the solution changed in color from white to dark blue or black. After the reaction, the solution was stored in a beaker in an ice bath to keep the solution cool, and then deionized (DI) water and HCl (35%, OCI) were sequentially added to adjust the pH to 7. Next, the solution was filtered with water and ethanol to remove the remaining Li^+, Cl^-, and EDA. After that, the filtered powder was dried in a vacuum oven for a few hours. For the control experiments, each single crystal structure of TiO_2, including only the anatase phase and only the rutile phase, were also prepared.

Characterization of the samples. To investigate the crystallinity of the rTiO_2 materials, including their crystal orientations and morphologies, the prepared samples were characterized by X-ray diffraction (XRD; Rigaku Ultima IV), transmission electron microscopy (TEM; JEOL JEM-2100F), and Raman spectroscopy with a laser wavelength of 532 nm. To investigate the energy bandgap properties and diffuse reflectance spectra, the UV-3600 and UV-VIS-NIR spectrophotometers (Shimadzu Corp.) were used. In addition, $BaSO_4$ was used as a standard. To investigate the chemical properties, X-ray photoelectron spectroscopy (XPS; ESCA 2000, VG Microtech) and electron spin resonance (ESR; X-band CW-EPR, QM09, RT, 2.97 mW, 9.64 GHz microwave frequency, 100 KHz modulation frequency, modulation amplitude: 1G, powder: 5 G, 10G ESR spectral data) measurements were obtained from the Korea Basic Science Institute in Seoul, Korea.

Photocatalytic degradation of algae. The investigation of the photocatalytic degradation of algae was carried out in petri dishes that each contained a 5-ml suspension of *Chlamydomonas segnis* (*Lobochlamys segnis,* NLP Co., Ltd.), in which the initial concentration was 7500 ± 10 cells/ml. Next, 10 mg (0.125 mmol) of

each TiO_2 sample in 20 ml of water were added and then stirred at room temperature (25 °C) for four hours while being irradiated by a UV lamp (300–500 nm, POWER ARC UV 100, UV Process Supply, Inc.) or solar simulator (150 Watt Ushio 150-MO Ozone Free Arc Lamp, HS Technologies). For every 30-min interval, 20 μl of the suspension was collected to monitor and analyze the cell conditions. The living algae cells showed random movement, but the dead algae did not move; instead, changes in the cell shapes and sizes were observed with an optical microscope (BiMeince Corp.) and a haemacytometer (Marienfeld-Superior) (Fig. 9). The living algae cells were counted three times for each sample to get the average number of cells. There were no changes in pH during the photocatalytic degradation.

References

1. Cooke, G. D. & Kennedy, R. H. Managing drinking water supplies. *Lake Reserv. Manage.* **17,** 157–174 (2001).
2. Shepherd, G. S. *et al.* Photocatalytic degradation of cyanobacterial microcystin toxins in water. *Toxicon* **36,** 1895–1901 (1998).
3. Peller, J. R. *et al.* TiO_2 as a photocatalyst for control of the aquatic invasive alga, cladophora, under natural and artificial light. *J. Photoch. Photobio A-Chem.* **186,** 212–217 (2007).
4. Hrudey, S. E., Hrudey, E. J. & Pollard, S. J. T. Risk management for assuring safe drinking water. *Environ. Int.* **32,** 948–957 (2006).
5. Hong, J. & Otaki, M. Association of photosynthesis and photocatalytic inhibition of algal growth by TiO_2. *J. Biosci. Bioeng.* **101,** 185–189 (2006).
6. Gladis, F. & Schumann, R. A suggested standardised method for testing photocatalytic inactivation of aeroterrestrial algal growth on TiO2-coated glass. *Int. Biodeter. Biodegr.* **65,** 415–422 (2011).
7. Lee, S. W., Obregón-Alfaro, S. & Rodríguez-González, V. Photocatalytic coatings of silver–TiO_2 nanocomposites on foamed waste-glass prepared by sonochemical process. *J. Photoch. Photobio. A-Chem.* **221,** 71–76 (2011).
8. Balcioglu, I. A., Arslan, I. & Sacan, M. T. Homogenous and heterogenous advanced oxidation of two commercial reactive dyes. *Environ. Technol.* **22,** 813–822 (2001).
9. Ndong, L. B. B. *et al.* Efficient dechlorination of chlorinated solvent pollutants under UV irradiation by using the synthesized TiO_2 nano-sheets in aqueous phase. *J. Environ. Sci.* **26,** 1188–1194 (2014).
10. Chen, C., Lei, P., Ji, H., Ma, W. & Zhao, J. Photocatalysis by titanium dioxide and polyoxometalate/TiO_2 cocatalysts. intermediates and mechanistic study. *Environ. Sci. Technol.* **38,** 329–337 (2004).
11. Javier, S. M. *et al.* Transformation products and reaction kinetics in simulated solar light photocatalytic degradation of propranolol using Ce-doped TiO_2. *Appl. Catal. B-Environ.* **129,** 13–29 (2013).
12. Foster, H. A., Ditta, I. B., Varghese, S. & Steele, A. Photocatalytic disinfection using titanium dioxide: spectrum and mechanism of antimicrobial activity. *Appl. Microbiol. Biot.* **90,** 1847–1868 (2011).
13. Linkous, C. A. *et al.* Photocatalytic inhibition of algae growth using TiO_2, WO_3, and cocatalyst modifications. *Environ. Sci. Technol.* **34,** 4754–4758 (2000).
14. Janus, M. & Morawski, A. W. New method of improving photocatalytic activity of commercial Degussa P25 for azo dyes decomposition. *Appl. Catal. B-Environ.* **75,** 118–123 (2007).
15. Zhang, Q., Wang, L., Feng, J., Xu, H. & Yan, W. Enhanced photoelectrochemical performance by synthesizing CdS decorated reduced TiO_2 nanotube arrays. *Phys. Chem. Chem. Phys.* **16,** 23431–23439 (2014).
16. Zhou, X. T., Ji, H. B. & Huang, X. J. Photocatalytic degradation of methyl orange over metalloporphyrins supported on TiO_2 degussa P25. *Molecules* **17,** 1149–1158 (2012).
17. Znad, H. & Kawase, Y. Synthesis and characterization of S-doped Degussa P25 with application in decolorization of Orange II dye as a model substrate. *J. Mol. Catal. A-Chem.* **314,** 55–62 (2009).
18. Yaghoubi, H. *et al.* Toward a visible light-driven photocatalyst: the effect of midgap-states-induced energy gap of undoped TiO_2 nanoparticles. *ACS Catal.* **5,** 327–335 (2015).
19. Fotiou, T., Triantis, T., Kaloudis, T. & Hiskia, A. Photocatalytic degradation of cylindrospermopsin under UV-A, solar and visible light using TiO_2. Mineralization and intermediate products. *Chemosphere* **119,** S89–S94 (2015).
20. Wang, Z. *et al.* H-doped black titania with very high solar absorption and excellent photocatalysis enhanced by localized surface plasmon resonance. *Adv. Funct. Mater.* **23,** 5444–5450 (2013).
21. Chen, X., Liu, L. & Huang, F. Black titanium dioxide (TiO_2) nanomaterials. *Chem. Soc. Rev.* **44,** 1861–1885 (2015).
22. Naldoni, A. *et al.* Effect of nature and location of defects on bandgap narrowing in black TiO_2 nanoparticles. *J. Am. Chem. Soc.* **134,** 7600–7603 (2012).
23. Zhao, Z. *et al.* Reduced TiO_2 rutile nanorods with well-defined facets and their visible-light photocatalytic activity. *Chem. Commun.* **50,** 2755–2757 (2014).
24. Guo, Y. *et al.* Effects of platinum on photo-assisted electrocatalytic activity of fringe-shaped highly ordered mesoporous titanium dioxide film. *J. Power Sources* **208,** 58–66 (2012).
25. Zhang, K. *et al.* An order/disorder/water junction system for highly efficient co-catalyst-free photocatalytic hydrogen generation. *Energy Environ. Sci.* **9,** 499–503 (2016).
26. Kang Q. *et al.* Reduced TiO_2 nanotube arrays for photoelectrochemical water splitting. *J. Mater. Chem. A* **1,** 5766–5774 (2013).
27. Wang, Z. *et al.* Visible-light photocatalytic, solar thermal and photoelectrochemical properties of aluminium-reduced black titania. *Energ. Environ. Sci.* **6,** 3007–3014 (2013).
28. Han, Z., Zhang, J., Yang, X., Zhu, H. & Cao, W. Synthesis and photoelectric property of poly(3-octylthiophene)/titanium dioxide hybrid. *J. Inorg. Organomet. P.* **20,** 32–37 (2010).
29. Han, Z., Zhang, J., Yang, X., Zhu, H. & Cao, W. Synthesis and photovoltaic property of poly(3-octylthiophene)/titanium dioxide/ferric oxide composite. *Synthetic Met.* **160,** 2167–2174 (2010).
30. Ebraheem, S. & El-Saied, A. Band gap determination from diffuse reflectance measurements of irradiated lead borate glass system doped with TiO_2 by using diffuse reflectance technique. *Mater. Sci. Appl.* **4,** 324–329 (2013).
31. Wodka, D. *et al.* Photocatalytic activity of titanium dioxide modified by Fe_2O_3 nanoparticles. *Appl. Surf. Sci.* **319,** 173–180 (2014).
32. Li, W. *et al.* Novel approach to enhance photosensitized degradation of rhodamine b under visible light irradiation by the $Zn_xCd_{1-x}S/TiO_2$ nanocomposites. *Environ. Sci. Technol.* **45,** 2987–2993 (2011).
33. Noda, H., Oikawa, K. & Kamada, H. ESR study of active oxygen radicals from photoexcited semiconductors using the spin-trapping technique. *Bull. Chem. Soc. Jpn.* **65,** 2505–2509 (1992).
34. Zheng, X. *et al.* Titanium dioxide photonic crystals with enhanced photocatalytic activity: matching photonic band gaps of TiO_2 to the absorption peaks of dyes. *J. Phys. Chem. C* **117,** 21263–21273 (2013).
35. Yan, Y. *et al.* Slightly hydrogenated TiO_2 with enhanced photocatalytic performance. *J. Mater. Chem. A* **2,** 12708–12716 (2014).
36. Yuangpho, N., Le, S. T. T., Treerujiraphapong, T., Khanitchaidecha, W. & Nakaruk, A. Enhanced photocatalytic performance of TiO_2 particles via effect of anatase–rutile ratio. *Physica E* **67,** 18–22 (2015).

Acknowledgements

This work was supported by the Center for Integrated Nanostructure Physics (CINAP), Institute for Basic Science (IBS) (IBS-R011-D1).

Author Contributions

All authors discussed the results and commented on the manuscript. H.L. designed the project. Y.K. and H.M.H. synthesized the samples. L.W. supervised the synthesis of the samples. Y.K. and I.K. performed the structural characterizations. Y.K. and Y.Y. performed the chemical characterizations. Y.K. performed and analyzed the algae disinfection experiments. Y.K. and H.L. co-wrote the manuscript.

Additional Information

Supplementary information accompanies this paper at http://www.nature.com/srep

Competing financial interests: The authors declare no competing financial interests.

How to cite this article: Kim, Y. *et al.* Solar-light photocatalytic disinfection using crystalline/amorphous low energy bandgap reduced TiO_2. *Sci. Rep.* **6**, 25212; doi: 10.1038/srep25212 (2016).